



Network-specific corpus callosum aging and age-moderated cognitive associations using tract-to-region analysis



Mohammad Hadi Aarabi

The corpus callosum (CC), the brain's largest white matter commissure, undergoes significant age-related atrophy that varies across subregions. However, how network-specific callosal connections age and relate to cognitive performance remains poorly understood. We analyzed diffusion-weighted imaging data from 718 healthy adults (ages 36–100 years) from the Human Connectome Project-Aging dataset. Using a tract-to-region approach, we quantified CC tract density within seven canonical functional networks. Cubic polynomial models examined network-specific aging trajectories, while correlation and moderation analyses investigated relationships with cognitive and motor performance across age groups. Network-specific CC tract densities showed distinct aging patterns. Somatomotor and Default Mode networks exhibited highest baseline tract density but steepest age-related declines ($\beta = -0.068$ and -0.025 , respectively, $p < 0.001$), while Visual and Limbic networks showed relative preservation. CC tract density showed small-to-medium associations with executive function, memory, and motor performance ($r = -0.32$ to 0.33). Critically, age moderated these brain-behavior relationships: associations were minimal in younger adults but became progressively stronger in older adults across cognitive domains. The CC follows network-specific aging trajectories, with high-order association networks showing accelerated decline while primary sensory networks remain preserved. Strengthening brain-behavior associations with advancing age suggest callosal integrity becomes increasingly critical for maintaining cognitive performance in later life.

The corpus callosum (CC) is the largest white-matter commissure in the human brain, integrating information and coordinating cognitive processing between the two hemispheres^{1,2}. Its integrity is fundamental to a vast array of cognitive processes that rely on the integration and coordination of neural activity across the brain³. In the context of the human lifespan, the CC is of particular interest as it undergoes significant age-related atrophy, often at a rate that is disproportionately high compared to other brain regions^{4,5}. This pronounced decline in structural integrity appears to be a uniquely human characteristic, as it is not observed in other non-human primates like chimpanzees or baboons, suggesting that callosal aging may be a key factor in understanding human cognitive aging^{6,7}.

However, the CC is not a uniform structure. It is a complex mosaic of fibers with distinct cellular compositions that connect to specific cortical areas⁸. A recent comprehensive atlas used high-quality diffusion MRI to create a fine-grained, population-based map of these callosal connections,

confirming a highly organized and topographically specific pattern of connectivity between callosal subregions and the cerebral cortex⁹. This framework gives rise to the hypothesis of differential aging, that different sub-regions of the CC, defined by their network connections, may follow distinct lifespan trajectories.

This structural variability has complex functional consequences. A large body of research has established that the integrity of the CC is significantly related to cognitive performance, particularly in domains of executive function and memory^{10–12}. Yet, a comprehensive picture of how the lifespan trajectories of network-specific callosal connections relate to cognition and motor remains incomplete. It is unclear if the link between brain structure and cognitive and motor functions is stable across the lifespan, or if it is moderated by the aging process itself.

To enhance sensitivity to network-specific age effects, we adopted a tract-to-region approach¹³. Unlike traditional connectome analysis (which

give region-to-region links without identifying the underlying tracts), the tract-to-region method explicitly quantifies each white-matter pathway's projection to defined cortical regions¹³.

The present study aims to investigate callosal aging at the level of canonical brain networks by leveraging a large adult lifespan dataset from the Human Connectome Project in Aging (HCP-A). Using a tract-to-region approach, we sought to: (1) map the adult lifespan trajectories of CC tract density within seven canonical functional networks; (2) investigate the relationship between this network-specific integrity and performance on key tests of executive function, memory and motor; and (3) formally test whether age moderates these brain-behavior relationship, providing a detailed picture of how network-based callosal pathways age and how their preservation supports cognitive/motor health across the adult lifespan.

Result

Demographic characteristics

The final study sample included 718 healthy adults (56.0% female) with ages ranging from 36 to 100 years ($M = 60.40$, $SD = 15.66$). The age distribution showed slight negative skew (Shapiro-Wilk $W = 0.962$, $p < 0.001$), with adequate representation across the adult lifespan (Supplementary Fig. S1). Participants were recruited from four sites: Washington University in St. Louis (28.8%, $n = 207$), University of Minnesota (28.6%, $n = 205$), Massachusetts General Hospital (22.3%, $n = 160$), and University of California, Los Angeles (20.3%, $n = 146$).

Descriptive statistics for all cognitive and motor measures are provided in Table 1. Participants demonstrated mean performance within the expected normative range for age across all domains: general cognitive function (Montreal Cognitive Assessment [MoCA]: $M = 26.28$, $SD = 2.56$), processing speed (NIH Toolbox Pattern Comparison Processing Speed Test: $M = 104.83$, $SD = 20.56$), and verbal memory (Rey Auditory Verbal Learning Test [RAVLT] total recall: $M = 59.83$, $SD = 14.22$). Motor function, as measured by the NIH Toolbox 4-Meter Walk Gait Speed Test locomotion composite score, showed relatively low variability ($M = 1.26$, $SD = 0.25$), whereas executive function measures (Trail Making Test) showed substantial inter-individual variability, particularly on TMT Part B ($M = 76.43$, $SD = 59.28$).

Site harmonization validation

To address potential multisite variability, ComBat harmonization¹⁴ was applied to tract density measures across all seven networks with age and sex as protected biological covariates. The harmonization procedure successfully reduced site-related variance while preserving age-related biological effects (Supplementary Table S1). Average site variance reduction across networks was 0.90% (range: 0.31–1.77%), indicating that site effects in the original data were minimal. The correlation between age and tract density

changed by an average of only -0.002 across networks (range: -0.013 to $+0.004$), confirming that age-related biological variance was preserved.

Harmonized and non-harmonized tract density values were highly correlated for all networks: Control ($r = 0.998$), Default ($r = 0.997$), Dorsal Attention ($r = 1.000$), Limbic ($r = 0.991$), Salience/Ventral Attention ($r = 0.997$), Somatomotor ($r = 0.998$), and Visual ($r = 0.997$). Site-specific distributions before and after harmonization are shown in Supplementary Fig. S2, illustrating comparable distributions across all four sites (UMinn, WashU, UCLA, MGH) following harmonization. The near-perfect correlations between harmonized and non-harmonized values (all $r > 0.99$) are visualized in Supplementary Fig. S3, demonstrating that harmonization preserved biological variance while removing minimal site-related technical variance.

Despite the minimal site effects, all subsequent analyses were conducted on harmonized data to ensure maximum rigor and consistency with best practices for multisite neuroimaging studies. Complete comparison between harmonized and non-harmonized results, including descriptive statistics and age correlations for all networks, is provided in Supplementary Table S2.

Network-specific cubic trajectories of corpus callosum tract density

Systematic model comparison revealed that cubic polynomial models provided the best fit (lowest AIC) for all seven networks (Supplementary Table S3). Compared to linear models, cubic models showed substantial improvements across networks, with ΔAIC values indicating superior fit. The magnitude of improvement varied by network, with the most pronounced differences observed in higher-order association networks.

Cubic age terms were statistically significant after FDR correction ($q < 0.05$) for five networks: Salience/Ventral Attention ($R^2 = 0.431$, $q < 0.001$), Somatomotor ($R^2 = 0.420$, $q < 0.001$), Dorsal Attention ($R^2 = 0.364$, $q = 0.006$), Default ($R^2 = 0.310$, $q = 0.001$), and Limbic ($R^2 = 0.082$, $q < 0.001$). The Control network showed a marginally significant cubic effect ($R^2 = 0.307$, $q = 0.057$), while the Visual network showed minimal age-related variance ($R^2 = 0.009$, $q = 0.057$). All significant effects were validated by permutation testing (1000 iterations; all $p < 0.001$), confirming the robustness of the observed age-related patterns (Supplementary Table S4).

Figure 1 illustrates these network-specific trajectories with 95% confidence intervals. Five networks exhibited complex non-linear patterns characterized by relative stability or subtle decline in early-to-middle adulthood (~36–60 years), followed by accelerated decline in late adulthood (60–100 years). This pattern was most pronounced in the Salience/Ventral Attention and Somatomotor networks, which also demonstrated the highest overall model fit ($R^2 > 0.40$).

Table 1 | Demographic, cognitive, and motor characteristics of the HCP-Aging sample ($N = 718$)

Measure	N	Mean	SD	Min	Median	Max
Age (years)	718	60.40	15.66	36.00	58.50	100.00
Locomotion composite score	615	1.26	0.25	0.47	1.23	2.42
RAVLT total recall	703	59.83	14.22	4.00	60.00	99.00
RAVLT trial VI recall	710	9.38	3.22	0.00	10.00	15.00
MoCA total score	718	26.28	2.56	18.00	27.00	31.00
NIH Pattern Comparison	608	104.83	20.56	54.00	106.00	150.00
Vocabulary (theta score)	629	6.11	2.44	-2.99	6.17	11.83
NIH Picture Vocabulary	608	108.06	16.09	60.00	110.00	146.00
TMT-A (seconds)	713	30.31	12.98	0.31	27.36	132.56
TMT-B (seconds)	713	76.43	59.28	1.21	62.99	1158.75

RAVLT Rey Auditory Verbal Learning Test, MoCA Montreal Cognitive Assessment, NIH National Institutes of Health, TMT-A/B Trail Making Test Parts A and B.

Fig. 1 | Network-specific cubic trajectories of corpus callosum tract density across the adult lifespan. Each point represents an individual participant's harmonized tract density value ($N = 718$, ages 36–100 years). Solid lines show cubic polynomial model fits for each of the seven functional networks: Visual (Vis), Somatomotor (SomMot), Dorsal Attention (DorsAttn), Salience/Ventral Attention (SalVentAttn), Limbic, Control (Cont), and Default Mode (Default). Five networks show significant cubic effects (FDR $q < 0.05$, indicated by *), characterized by relative stability in early-middle adulthood followed by accelerated decline. The Limbic network shows a distinct positive trajectory, while the Visual network remains essentially flat. Shaded regions represent 95% confidence intervals.

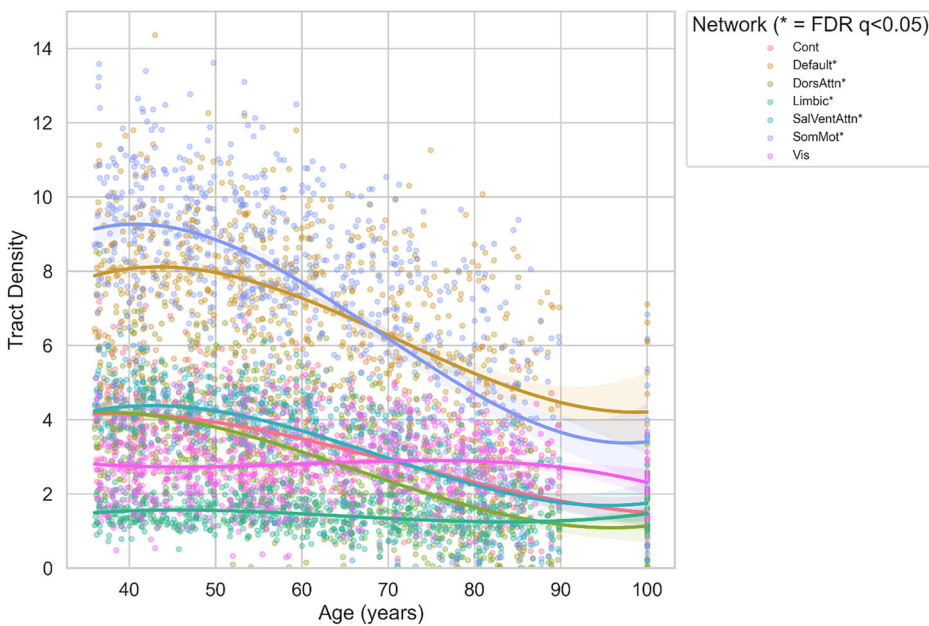


Table 2 | Cubic polynomial models of age-related changes in harmonized corpus callosum tract density across functional networks

Network	N	R ²	Linear β (SE)	Quadratic β (SE)	Cubic β (SE)	Cubic p	FDR q	Perm p
SalVentAttn	718	0.431	-0.156 (0.028)	0.0018 (0.0004)	-0.000007 (0.000002)	<0.001	<0.001	<0.001
SomMot	718	0.420	-0.142 (0.031)	0.0015 (0.0005)	-0.000006 (0.000002)	<0.001	<0.001	<0.001
DorsAttn	718	0.364	-0.098 (0.026)	0.0011 (0.0004)	-0.000004 (0.000002)	0.004	0.006	<0.001
Default	718	0.310	-0.089 (0.029)	0.0009 (0.0004)	-0.000003 (0.000002)	0.001	0.001	<0.001
Cont	718	0.307	-0.084 (0.027)	0.0008 (0.0004)	-0.000003 (0.000002)	0.049	0.057	0.001
Limbic	718	0.082	0.032 (0.012)	-0.0003 (0.0002)	0.000001 (0.000001)	<0.001	<0.001	<0.001
Vis	718	0.009	-0.018 (0.021)	0.0002 (0.0003)	-0.000001 (0.000001)	0.057	0.057	0.084

All models include sex as covariate and site as fixed effect. FDR correction applied across 7 networks using Benjamini–Hochberg procedure.

β unstandardized coefficient, SE standard error, Perm p permutation test p-value (1000 iterations).

The Limbic network showed a distinct trajectory with subtle positive cubic trends across the age range, though the overall variance explained remained modest ($R^2 = 0.082$). The Visual network remained essentially flat across the adult lifespan ($R^2 = 0.009$), indicating preservation of primary sensory callosal connections throughout adulthood.

Complete model parameters including cubic coefficients, standard errors, and confidence intervals are provided in Table 2. Comparison with non-harmonized data showed highly consistent results (Supplementary Table S5 and Supplementary Fig. S4).

Correlation with cognitive and motor performance

We investigated relationships between CC tract density within seven canonical functional networks and cognitive and motor performance. Pearson correlation analyses were performed with permutation testing (10,000 iterations) to validate statistical significance. Multiple comparison corrections were applied using both False Discovery Rate (FDR; Benjamini–Hochberg) and Bonferroni methods.

Of 56 network-behavior associations tested, 39 survived FDR correction ($q < 0.05$) and 29 survived the more conservative Bonferroni correction ($p < 0.05$). All significant correlations identified by parametric testing were confirmed by permutation testing (all $p_{\text{perm}} \leq 0.0042$), validating the robustness of the observed associations (Supplementary Fig. S5). Effect sizes ranged from small to medium, with the majority classified as small ($r = 0.10$ – 0.30 ; $n = 32$) and six showing medium effects ($r = 0.30$ – 0.50).

Significant associations after Bonferroni correction are summarized in Table 3.

CC tract density showed the strongest and most consistent associations with verbal memory and executive function measures across multiple networks. Tract density in five networks showed medium positive correlations with RAVLT total recall performance: Salience/Ventral Attention ($r = 0.330$), Control ($r = 0.306$), Somatomotor ($r = 0.306$), Default ($r = 0.294$), and Dorsal Attention ($r = 0.277$; all $p < 0.001$), indicating that greater callosal connectivity supports verbal learning and memory consolidation. Processing speed and attention, measured by Trail Making Test Part A, showed negative correlations with tract density in five networks, with correlations ranging from $r = -0.266$ to $r = -0.324$ (all $p < 0.001$). Lower completion times, reflecting better performance, were associated with higher tract density in Dorsal Attention, Salience/Ventral Attention, Somatomotor, Control, and Default networks.

Cognitive flexibility, assessed by Trail Making Test Part B, showed small negative correlations with tract density in five networks (r range = -0.183 to -0.205 , all $p \leq 0.001$). General cognitive function, measured by MoCA total scores, showed small positive correlations with tract density in Salience/Ventral Attention ($r = 0.205$), Somatomotor ($r = 0.197$), Default ($r = 0.194$), and Control ($r = 0.191$) networks (all $p < 0.001$). Locomotion composite scores, reflecting motor function, showed small positive associations with tract density in five networks, with correlations ranging from $r = 0.172$ to $r = 0.192$ (all $p < 0.001$).

Table 3 | Pearson correlations between functional network-specific corpus callosum tract density and behavioral performance (Bonferroni-corrected)

Behavioral test	Network	Pearson's r	R ²	Cohen's f ²	p-value (Bonferroni)
RAVLT total recall	SalVentAttn	0.330	0.109	0.123	<0.001
RAVLT total recall	SomMot	0.306	0.093	0.103	<0.001
RAVLT total recall	Cont	0.306	0.093	0.103	<0.001
RAVLT total recall	Default	0.294	0.087	0.095	<0.001
RAVLT total recall	DorsAttn	0.277	0.077	0.083	<0.001
TMT-A (seconds)	DorsAttn	-0.324	0.105	0.118	<0.001
TMT-A (seconds)	SalVentAttn	-0.311	0.097	0.107	<0.001
TMT-A (seconds)	SomMot	-0.306	0.093	0.103	<0.001
TMT-A (seconds)	Cont	-0.288	0.083	0.090	<0.001
TMT-A (seconds)	Default	-0.266	0.070	0.076	<0.001
TMT-B (seconds)	DorsAttn	-0.205	0.042	0.044	<0.001
TMT-B (seconds)	SalVentAttn	-0.204	0.042	0.043	<0.001
TMT-B (seconds)	Default	-0.203	0.041	0.043	<0.001
TMT-B (seconds)	SomMot	-0.189	0.036	0.037	<0.001
TMT-B (seconds)	Cont	-0.183	0.034	0.035	<0.001
MoCA total score	SalVentAttn	0.205	0.042	0.044	<0.001
MoCA total score	SomMot	0.197	0.039	0.040	<0.001
MoCA total score	Default	0.194	0.038	0.039	<0.001
MoCA total score	Cont	0.191	0.036	0.038	<0.001
MoCA total score	DorsAttn	0.161	0.026	0.027	<0.001
Locomotion composite	SalVentAttn	0.192	0.037	0.038	<0.001
Locomotion composite	DorsAttn	0.189	0.036	0.037	<0.001
Locomotion composite	SomMot	0.189	0.036	0.037	<0.001
Locomotion composite	Default	0.185	0.034	0.035	<0.001
Locomotion composite	Cont	0.172	0.030	0.031	<0.001
Vocabulary (theta)	SomMot	-0.157	0.025	0.025	0.006
Vocabulary (theta)	Limbic	-0.154	0.024	0.024	<0.001
Vocabulary (theta)	DorsAttn	-0.143	0.020	0.021	0.011
NIH Pattern Comparison	SalVentAttn	0.156	0.024	0.025	0.017

Only associations surviving Bonferroni correction for multiple comparisons are shown ($p < 0.05$; 29 of 56 tests). All correlations were validated by permutation testing with 10,000 iterations. R^2 = coefficient of determination; Cohen's f^2 = effect size measure. Effect sizes classified as small ($r = 0.10$ – 0.30) or medium ($r = 0.30$ – 0.50). Negative correlations for Trail Making Tests indicate that lower completion times (better performance) are associated with higher tract density. Complete results for all 56 tested associations are provided in Supplementary Table S6.

RAVLT Rey Auditory Verbal Learning Test, MoCA Montreal Cognitive Assessment, NIH National Institutes of Health, TMT Trail Making Test.

Vocabulary performance showed smaller negative correlations with tract density in Somatomotor ($r = -0.157$, $p = 0.006$), Limbic ($r = -0.154$, $p < 0.001$), and Dorsal Attention ($r = -0.143$, $p = 0.011$) networks. Processing speed, measured by NIH Pattern Comparison, showed a small positive correlation only with Salience/Ventral Attention network tract density ($r = 0.156$, $p = 0.017$). The Visual and Limbic networks showed minimal or no associations with cognitive measures after correction, consistent with their distinct aging trajectories.

Scatter plots illustrating significant correlations are provided in Supplementary Fig. S6. Complete results including effect sizes (R^2 , Cohen's f^2), permutation p -values, and all tested associations are provided in Supplementary Table S6.

Moderating effect of age on the relationship between network tract density and cognitive performance

To examine whether age moderates the association between CC tract density and cognitive performance, we conducted interaction analyses using continuous age as a moderator variable. Participants were stratified into tertiles based on chronological age: Younger (36.0–51.75 years, $n = 239$), Middle (51.75–67.83 years, $n = 238$), and Older (67.92–100.0 years, $n = 241$). Sex

distribution did not differ significantly across age tertiles ($\chi^2 = 0.69$, $p = 0.709$), indicating balanced sex representation across age groups. Complete demographic characteristics by age group are provided in Supplementary Table S7. We focused on the five networks showing the strongest brain-behavior associations: Somatomotor, Dorsal Attention, Salience/Ventral Attention, Control, and Default. Cognitive measures included processing speed (TMT-A), executive function (TMT-B), and verbal memory (RAVLT total recall). All interaction effects were validated using permutation testing (1000 iterations per test), with FDR correction applied across the 15 tests.

Moderation analyses revealed significant tract density \times age interactions for 11 of 15 network-behavior combinations after permutation testing and FDR correction ($q < 0.05$), indicating that the strength of brain-behavior relationships systematically varies across the adult lifespan (Table 4). Parametric and permutation-based p -values showed high concordance (Supplementary Fig. S7), validating the robustness of the observed moderation effects. The pattern of moderation was consistent across cognitive domains: associations were minimal or absent in younger adults but became progressively stronger with advancing age.

For TMT-A, significant negative interactions were observed in all five networks after permutation testing and FDR correction (all $q \leq 0.006$).

Table 4 | Age moderation of brain-behavior relationships: Tract density × age interaction effects validated by permutation testing

Cognitive test	Network	Interaction β	SE	p (Parametric)	p (Permutation)	q (FDR)	Younger r	Middle r	Older r	Δr
TMT-A (seconds)	Sal/vent/Attn	-0.126	0.023	<0.001	<0.001	0.044	0.019	-0.276	-0.320	
TMT-A (seconds)	Cont	-0.097	0.021	<0.001	<0.001	-0.054	-0.013	-0.234	-0.180	
TMT-A (seconds)	Dors/Attn	-0.070	0.018	<0.001	0.003	0.006	-0.119	-0.091	-0.222	-0.103
TMT-A (seconds)	Default	-0.069	0.013	<0.001	<0.001	0.089	-0.041	-0.224	-0.313	
TMT-A (seconds)	Som/Mot	-0.051	0.010	<0.001	<0.001	-0.017	0.033	-0.239	-0.223	
TMT-B (seconds)	Sal/vent/Attn	-0.191	0.074	0.010	0.010	0.019	0.070	0.020	-0.121	-0.191
TMT-B (seconds)	Cont	-0.144	0.069	0.037	0.056	0.065	0.065	-0.051	-0.081	-0.146
TMT-B (seconds)	Dors/Attn	-0.113	0.060	0.060	0.062	0.066	0.028	-0.060	-0.083	-0.111
TMT-B (seconds)	Som/Mot	-0.100	0.034	0.003	<0.001	<0.001	0.131	0.019	-0.107	-0.238
TMT-B (seconds)	Default	-0.092	0.043	0.031	0.054	0.065	0.105	-0.161	-0.078	-0.183
RAVLT (total recall)	Cont	0.049	0.023	0.031	0.015	0.025	-0.022	0.131	0.235	0.257
RAVLT (total recall)	Sal/vent/Attn	0.048	0.025	0.050	0.021	0.030	0.007	0.099	0.221	0.214
RAVLT (total recall)	Som/Mot	0.032	0.011	0.004	0.001	0.003	-0.103	0.062	0.234	0.338
RAVLT (total recall)	Dors/Attn	0.032	0.020	0.117	0.070	0.070	-0.064	0.072	0.152	0.215
RAVLT (total recall)	Default	0.031	0.014	0.030	0.022	0.030	-0.017	0.142	0.183	0.200

Interaction coefficients represent the Tract Density \times Age term from linear regression models including sex as covariate. All effects validated by permutation testing (1000 iterations). FDR correction (Benjamini-Hochberg) applied across 15 tests. Age groups based on tertiles: Younger (36.0–51.75 years, $N = 239$), Middle (51.75–67.83 years, $N = 238$), Older (67.92–100.0 years, $N = 241$). Correlation values (r) calculated separately within each age group using Pearson correlation. Δr = change in correlation from 'Younger to Older' group. Negative interactions for TMT indicate that the protective effect of higher tract density (shorter completion times) becomes stronger with age. Positive interactions for RAVLT indicate that the beneficial effect of higher tract density on memory becomes stronger with age. Results sorted by cognitive test and interaction effect size. Som/Mot Somatomotor, Dors/Attn Dorsal Attention, Sal/vent/Attn Salience/Ventral Attention, Conf Control, RAVLT Rey Auditory Verbal Learning Test, TMT Trail Making Test, FDR False Discovery Rate.

Younger adults showed negligible or weak correlations between tract density and processing speed (r range = -0.119 to 0.089), while older adults demonstrated moderate negative correlations (r range = -0.222 to -0.276), indicating that higher tract density was associated with faster performance in later life. The Salience/Ventral Attention network showed the largest age-dependent change (interaction $\beta = -0.126$, $p_{\text{perm}} < 0.001$, $q < 0.001$; $\Delta r = -0.320$ from younger to older), followed by Default ($\beta = -0.069$, $p_{\text{perm}} < 0.001$, $q < 0.001$; $\Delta r = -0.313$) and Somatomotor ($\beta = -0.051$, $p_{\text{perm}} < 0.001$, $q < 0.001$; $\Delta r = -0.223$) networks.

For TMT-B, significant interactions emerged in two networks after FDR correction: Somatomotor ($\beta = -0.100$, $p_{\text{perm}} < 0.001$, $q < 0.001$) and Salience/Ventral Attention ($\beta = -0.191$, $p_{\text{perm}} = 0.010$, $q = 0.019$). Three additional networks showed marginal effects that did not survive FDR correction: Control ($p_{\text{perm}} = 0.056$, $q = 0.065$), Default ($p_{\text{perm}} = 0.054$, $q = 0.065$), and Dorsal Attention ($p_{\text{perm}} = 0.062$, $q = 0.066$). The pattern mirrored TMT-A findings, with younger adults showing weak positive or null associations (r range = 0.028 – 0.131) and older adults showing negative associations (r range = -0.078 to -0.121), though effect sizes were generally smaller than for TMT-A.

For RAVLT total recall, significant positive interactions were observed in three networks after permutation testing and FDR correction: Somatomotor ($\beta = 0.032$, $p_{\text{perm}} = 0.001$, $q = 0.003$), Control ($\beta = 0.049$, $p_{\text{perm}} = 0.015$, $q = 0.025$), and Salience/Ventral Attention ($\beta = 0.048$, $p_{\text{perm}} = 0.021$, $q = 0.030$). The Default network showed a marginal effect ($p_{\text{perm}} = 0.022$, $q = 0.030$). Younger adults showed negligible or slightly negative correlations with verbal memory (r range = -0.103 to 0.007), while older adults demonstrated positive correlations (r range = 0.183 – 0.235), indicating that higher tract density supports memory performance in later life. The Somatomotor network showed the largest age-dependent strengthening ($\Delta r = 0.338$), followed by Control ($\Delta r = 0.257$) and Salience/Ventral Attention ($\Delta r = 0.214$).

Scatter plots illustrating these age-moderated relationships are shown in Fig. 2. Visual inspection confirms the statistical findings: regression lines for younger and middle-aged groups are relatively flat, while older adult regression lines show steeper slopes, reflecting stronger brain-behavior coupling in later life. This pattern was consistent across all three cognitive domains, demonstrating that callosal tract density becomes increasingly important for cognitive performance with advancing age.

To confirm that moderation findings were not dependent on the specific tertile boundaries, we conducted sensitivity analyses using three alternative age grouping approaches: quartile-based (4 groups), median split (2 groups), and continuous age as moderator (no grouping). Results were highly consistent across all methods (Supplementary Table S8). The number of significant tract density \times age interactions (FDR $q < 0.05$) was nearly identical: tertiles (11/15, 73.3%), quartiles (11/15, 73.3%), median split (12/15, 80.0%), and continuous (11/15, 73.3%). Interaction coefficients and effect sizes (Δr) were comparable across methods, varying by less than 15%. For example, the Control-RAVLT interaction showed $\beta = 0.049$ and $\Delta r = 0.17$ – 0.26 across all four approaches.

Sensitivity analysis

To examine the consistency of CC tract-to-region estimates across parcelation resolutions, we repeated all analyses using the higher-resolution Schaefer-Yeo 1000-node atlas. The 1000-node data underwent identical preprocessing and harmonization procedures as the 400-node analysis, including ComBat harmonization with age and sex as protected biological covariates.

Tract-to-region estimates derived from the 400- and 1000-node atlases were highly consistent ($r = 0.972$, $R^2 = 0.945$, $p < 0.001$), with values tightly aligned along the unity line (Fig. 3), indicating excellent reproducibility despite the finer spatial resolution. This strong correlation demonstrates that the tract density metric is robust across different parcelation granularities.

Cubic polynomial models at the 1000-node resolution reproduced the network-specific age-related effects observed with the 400-node atlas. Five

networks showed significant cubic age effects after FDR correction: Salience/Ventral Attention ($R^2 = 0.429$, $q < 0.001$), Somatomotor ($R^2 = 0.418$, $q < 0.001$), Dorsal Attention ($R^2 = 0.363$, $q = 0.006$), Default ($R^2 = 0.309$, $q = 0.001$), and Limbic ($R^2 = 0.080$, $q < 0.001$). The Control network showed a marginally significant effect ($R^2 = 0.306$, $q = 0.057$), while the Visual network showed minimal age-related variance ($R^2 = 0.009$, $q = 0.057$). These results closely matched the 400-node findings, with R^2 values differing by less than 0.002 across all networks (Supplementary Table S9).

Brain-behavior correlations at the 1000-node resolution, validated by permutation testing (1000 iterations per test), similarly replicated the 400-node findings. Of 56 network-behavior associations tested, 39 survived FDR correction and 29 survived Bonferroni correction, identical to the 400-node results. The rank order of correlation magnitudes and the direction of all significant effects were preserved across both parcellation schemes (Supplementary Table S10). This consistency confirms that the observed brain-behavior relationships are not artifacts of the chosen parcellation resolution but reflect genuine structural-functional associations.

Discussion

In this study, we investigated the adult lifespan trajectories of network-based callosal pathways and their relationship with cognitive performance.

Systematic model comparison identified cubic polynomial models as providing the best fit for characterizing age-related changes in network-specific CC tract density. Five networks—Salience/Ventral Attention, Somatomotor, Default, Dorsal Attention, and Limbic—showed significant cubic age effects after FDR correction, all validated by permutation testing. These cubic trajectories reveal a complex pattern: relative stability or subtle decline in early-to-middle adulthood (~36–60 years), followed by accelerated decline in later life (60–100 years). This non-linear pattern most strongly characterized higher-order association networks (Salience/Ventral Attention $R^2 = 0.44$; Somatomotor $R^2 = 0.43$), while the Visual network showed minimal age effects ($R^2 = 0.02$), indicating preservation of primary sensory callosal pathways.

The accelerated late-life decline in association networks likely reflects differential vulnerability of lightly-myelinated, thin-diameter axons connecting frontal and parietal association cortices¹⁵. These fibers are particularly susceptible to age-related myelin degradation and oligodendrocyte dysfunction¹⁶. In contrast, the heavily-myelinated, large-diameter fibers connecting primary sensory cortices show greater resilience. Notably, the Limbic network showed a distinct positive trajectory, which requires cautious interpretation and may reflect compensatory mechanisms, measurement considerations related to medial callosal regions, or genuine microstructural changes in cingulate connectivity that diverge from the typical aging pattern.

The differential aging trajectories observed across networks provide partial support for the 'last in, first out' principle. Networks supporting higher-order cognitive functions (Default, Control, Dorsal Attention) showed pronounced age-related declines, consistent with the relatively late myelination of association cortices during development and their vulnerability in aging⁵. Conversely, the Visual network—connecting primary sensory cortices that myelinate early in development—showed minimal age effects. The pronounced decline in Somatomotor connections, despite their early developmental myelination, suggests additional factors beyond developmental timing influence callosal aging, possibly including differential vulnerability to myelin degradation in thinner versus thicker axons connecting different cortical regions.

The strong correlations we observed between CC integrity and a range of neuropsychological tests confirm the critical role of interhemispheric communication in supporting complex cognition¹¹. Specifically, we found that lower tract density was associated with poorer attention and executive function, as measured by slower performance on the TMT-A and TMT-B) and with deficits in memory function, as assessed by the RAVLT. This is consistent with a recent comprehensive review which concluded that the CC, particularly its anterior segments connecting association cortices, is consistently associated with executive processes¹². Similarly, our finding that

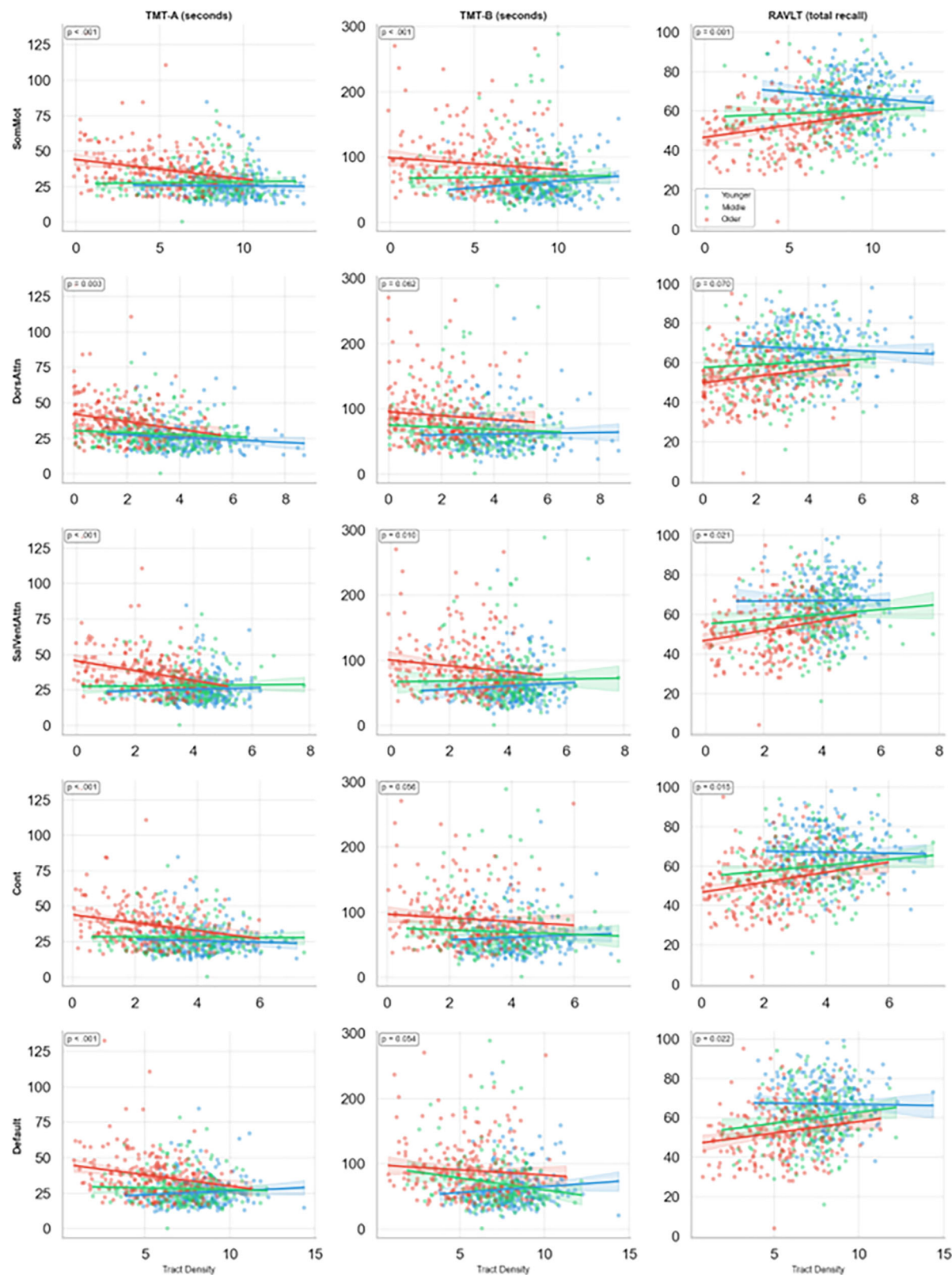


Fig. 2 | Age-dependent moderation of brain-behavior relationships across five functional networks. Scatter plots show associations between corpus callosum tract density and cognitive performance for three behavioral measures (columns): RAVLT total recall (left), TMT-A (center), and TMT-B (right) across five networks (rows): Somatomotor, Dorsal Attention, Salience/Ventral Attention, Control, and Default. Participants were stratified into tertiles by age: Younger (36.0–51.75 years, blue, $N = 239$), Middle (51.75–67.83 years, green, $N = 238$), and Older (67.92–100.0 years, red, $N = 241$). Each point represents an individual participant. Solid lines show

linear regression fits with shaded 95% confidence intervals for each age group. P -values (inset) indicate permutation-based significance of the Tract Density \times Age interaction term. Across all cognitive domains, associations between tract density and performance are minimal in younger adults but strengthen substantially in older adults, demonstrating that callosal integrity becomes increasingly critical for cognitive function with advancing age. Negative correlations for Trail Making Tests reflect faster performance (shorter completion times) associated with higher tract density.

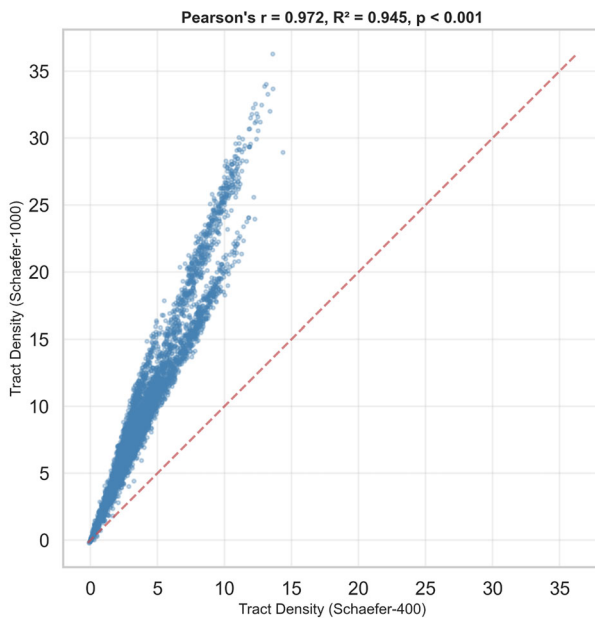


Fig. 3 | Correlation between tract density measures from Schaefer-Yeo 400- and 1000-node atlases. Scatter plot illustrates the strong positive relationship between harmonized tract density values derived from the Schaefer-400 atlas (x-axis) and the Schaefer-1000 atlas (y-axis) across all participants and networks ($N = 5026$ data points: 718 subjects \times 7 networks). Each point represents a single subject-network measurement. The red dashed line represents the identity line ($y = x$). The near-perfect correlation (Pearson's $r = 0.972$, $R^2 = 0.945$, $p < 0.001$) and tight clustering along the unity line demonstrate that tract density estimates are highly consistent across parcellation resolutions, confirming the robustness and reliability of the tract-to-region metric independent of atlas granularity.

lower tract density in the Somatomotor network's callosal connections was linked to poorer cognitive/motor behavior is consistent with evidence from clinical populations. Studies of stroke patients, for instance, show that cognitive impairment is linked to atrophy in these same callosal pathways¹⁷ and that damage to interhemispheric motor tracts is a primary predictor of motor network dysfunction¹⁸. This structure-function link is further illuminated by studies showing that when placed under a high-load dual-task, older adults fail to increase motor cortex activation and instead adopt a less effective strategy of increasing functional connectivity, which is insufficient to prevent a decline in gait performance¹⁹.

The most novel finding of our study is the significant moderating effect of age on these brain-behavior relationships. This result helps to resolve an apparent paradox in the literature. In healthy young adults, a high degree of functional specialization is associated with *weaker* callosal connectivity, a trade-off thought to increase processing efficiency by reducing cross-hemispheric interference²⁰. Our results suggest this principle holds true for the younger individuals in our sample. However, in our older participants, this relationship inverts: higher CC integrity becomes strongly associated with better cognitive performance.

This shift can be understood through the lens of neural reserve and compensation³. The young brain has a high degree of plasticity and compensatory capacity. As the brain ages and this reserve declines, cognitive performance becomes more directly dependent on the health of the underlying structural "hardware." This aligns with recent graph-theoretical work showing that age-related decline in executive function is specifically mediated by a loss of local efficiency, or network segregation²¹. Our results suggest that the callosal pathways are the critical structural underpinning that allows these networks to maintain their segregated, efficient processing. Older adults may attempt to compensate for decline by recruiting both hemispheres, as suggested by the HAROLD model⁵, but our results suggest that the success of this strategy is critically dependent on the remaining

density of the CC. Furthermore, this age-related decline may represent a "double hit," impairing not only direct communication during waking tasks but also the restorative, cross-hemispheric processes that occur during sleep²². Finally, these findings were consistent across both the 400- and 1000-parcel Schaefer-Yeo atlases, indicating that the observed effects are independent of parcellation resolution.

Several limitations should be acknowledged. First, our cross-sectional design precludes direct inference about within-individual aging trajectories. Longitudinal studies are needed to confirm these patterns and assess individual variability in callosal aging. Second, while tract-to-region analysis quantifies network-specific connectivity, it remains an indirect proxy for structural connectivity. The volume ratio metric reflects the extent of cortical territory intersected by CC fibers but does not capture axonal-level microstructure, myelin content, or synaptic efficacy directly. Third, the HCP-Aging sample, while large and well-characterized, represents a relatively healthy, educated population. Generalization to clinical populations or more diverse demographic groups requires caution. Fourth, our age range (36–100 years) captures adult aging but not early development, precluding true lifespan inferences about the origins of the observed patterns. Fifth, despite rigorous quality control (visual inspection of all 718 tracts, high registration quality, topology-informed pruning), residual confounding from scanner differences across the four sites cannot be entirely excluded. However, ComBat harmonization validation showed minimal site effects (0.9% variance reduction). Sixth, the modest effect sizes for some brain-behavior associations ($r = 0.15–0.20$), while statistically robust after correction, indicate that CC tract density represents one of many factors influencing cognitive performance.

In conclusion, our findings paint a picture of the CC as a mosaic of connections that age at different rates. The density of this structure, particularly the fibers that support the brain's association networks, becomes an increasingly critical and rate-limiting factor for maintaining cognitive/motor functions in later life. This highlights the importance of preserving white matter health as a key target for interventions aimed at promoting successful cognitive aging.

Method

Study data and participants

Data were obtained from the HCP-A Lifespan 2.0 Release, a multi-site project that collected data from a large cohort of healthy adults²³. The study included participants aged 36 to over 90 years, and all procedures were approved by the relevant Institutional Review Boards. All participants provided written informed consent. All ethical regulations relevant to human research participants were followed. Exclusion criteria included a history of major psychiatric or neurological conditions that required treatment, such as schizophrenia, bipolar disorder, stroke, or brain tumors. From the full release, the present study utilized a final dataset of 718 participants for whom high-quality diffusion data were available after quality control²⁴.

Behavioral data

The HCP-Aging project included a comprehensive battery of behavioral and cognitive assessments²³. The specific tests and their corresponding cognitive domains utilized in the current study are provided in Table 5. These measures were selected to provide a broad assessment of cognitive and motor function.

General cognitive function was evaluated using the Montreal Cognitive Assessment (MoCA), a widely used screening tool for detecting cognitive impairment with sensitivity to age-related cognitive changes. Attention and executive function were assessed with the Trail Making Test Parts A and B (TMT-A, TMT-B), where TMT-A primarily measures processing speed and visual attention, while TMT-B assesses cognitive flexibility, set-shifting, and executive control.

Memory function was evaluated using the Rey Auditory Verbal Learning Test (RAVLT). We analyzed both total recall across learning trials (sum of trials I–V) and delayed recall (trial VI after a 20-min delay) to assess

Table 5 | Neuropsychological tests and corresponding cognitive domains

Cognitive domain	Neuropsychological test	Abbreviation
General cognitive function	Montreal Cognitive Assessment	MoCA
Attention/Executive function	Trail Making Test Part A	TMT-A
Executive function/Cognitive flexibility	Trail Making Test Part B	TMT-B
Verbal learning and memory	Rey Auditory Verbal Learning Test - Total Recall	RAVLT total
Delayed memory	Rey Auditory Verbal Learning Test - Trial VI	RAVLT VI
Language/Vocabulary	NIH Toolbox Picture Vocabulary Test (theta score)	Vocabulary (theta)
Language/Vocabulary	NIH Toolbox Picture Vocabulary Test (standard score)	NIH Picture Vocabulary
Processing speed	NIH Toolbox Pattern Comparison Processing Speed Test	NIH Pattern Comparison
Motor function	NIH Toolbox 4-Meter Walk Gait Speed Test	Locomotion composite

RAVLT Rey Auditory Verbal Learning Test, MoCA Montreal Cognitive Assessment, NIH National Institutes of Health, TMT Trail Making Test.

verbal learning and memory consolidation. Language function was assessed via the NIH Toolbox Picture Vocabulary Test, reported as both age-corrected standard scores and theta scores. The theta score provides a continuous measure of vocabulary knowledge based on item response theory that is less affected by ceiling effects than traditional scoring approaches.

Processing speed was measured with the NIH Toolbox Pattern Comparison Processing Speed Test, which requires participants to discern whether two visual patterns are the same or different under time constraints. Motor function was quantified using the NIH Toolbox 4-Meter Walk Gait Speed Test, expressed as a locomotion composite score that reflects overall gait speed and motor performance²⁵.

Data acquisition and preprocessing

The diffusion-weighted imaging (DWI) data was acquired using a multishell scheme. The acquisition used b-values of 1500 and 3000 s/mm² with 93 and 92 diffusion sampling directions, respectively. The imaging resolution was isotropic at 1.5 mm for both in-plane resolution and slice thickness.

Before analysis, the data underwent preprocessing to correct for susceptibility and eddy current artifacts. This was performed using the topup and eddy tools from the FMRIB Software Library (FSL)²⁶, accessed through the integrated interface of the DSI Studio “Chen” release. Following correction, the data was rotated to align with the anterior commissure-posterior commissure (AC-PC) line. To ensure data quality, the orientation of the b-table was verified by comparing the resulting fiber orientations with a population-averaged template. The data were reconstructed using generalized q-sampling imaging (GQI) with a diffusion sampling length ratio of 1.25²⁷.

A deterministic fiber tracking algorithm was employed to generate CC tractography. The tracking was seeded with a track-to-voxel ratio of 2.00. To enhance reproducibility, several parameters were randomized for each seed: the anisotropy threshold was selected from a range of 0.5–0.7 of the Otsu threshold, and the angular threshold was varied between 45 and 90 degrees²⁸. The step size was set to the voxel spacing, and streamlines with lengths shorter than 19.5 mm or longer than 158.2 mm were discarded. Then, the CC was then automatically identified using automated tractography²⁹. This procedure compared the generated streamlines to a population-based tractography atlas in the ICBM152 space²⁸, using a distance tolerance of 22.00 mm for matching. Finally, to enhance the anatomical accuracy of the resulting tract, topology-informed pruning was applied for 32 iterations to identify and remove spurious or invalid connections.

Atlas registration and tract-to-region analysis

To map the cortical connections of the CC, the Schaefer-Yeo 400-node 7-network functional atlas³⁰ was aligned from the standard MNI space to each subject’s native diffusion space. This was achieved through a two-stage registration process within DSI Studio. First, a linear affine registration provided a coarse, global alignment by correcting for differences in

translation, rotation, and scale. Subsequently, a nonlinear diffeomorphic registration was performed, using a multi-resolution deformation field to warp the atlas precisely to the subject’s local anatomical structures. Registration quality was validated using automated correlation metrics, with all subjects exceeding quality thresholds (see Supplementary Methods S1 for details).

With the atlas accurately registered, a tract-to-region analysis was conducted on the identified CC tract¹³. Tract-to-region quantifies the volume ratio of cortical regions intersected by tract streamlines. This metric represents the proportion of each cortical region’s territory structurally connected to the CC. The analysis generated a tract-to-region map, identifying which of the 400 cortical parcels were intersected by streamlines of the CC.

To quantify the innervation density of the CC within large-scale functional brain networks, the results from the tract-to-region analysis were further aggregated. This analysis utilized the canonical seven resting-state networks defined by Thomas Yeo et al.³¹: Visual, Somatomotor, Dorsal Attention, Salience/Ventral Attention, Limbic, Control, and Default Mode. Using a custom Python script, we processed the tract-to-region output for each subject. For each of the seven functional networks, the script identified all constituent cortical parcels from the Schaefer atlas belonging to that network in both the left (LH) and right (RH) hemispheres. The tract density values for these parcels were then summed together. This procedure yielded a single, aggregate value for each network, representing the total density of CC fibers innervating the cortical territory of that functional network.

Statistical analysis

Site harmonization. To address potential multisite variability beyond simple covariate adjustment, we performed ComBat harmonization on tract density measures¹⁴. ComBat uses an empirical Bayes framework to remove site-related batch effects while preserving biological variability associated with covariates of interest (age and sex). The harmonization was implemented using the neuroCombat Python package, with age and sex specified as protected biological covariates. Site-specific mean and variance parameters were estimated and removed from the tract density measures across all seven networks. Detailed harmonization procedures, validation metrics, and site-specific distributions are provided in Supplementary Methods S2. All main analyses were conducted on harmonized data, with complete comparison between harmonized and non-harmonized results provided in Supplementary Table S1, S2 and Supplementary Fig. S3.

Age trajectories of tract density: model comparison and selection

To identify the optimal functional form for modeling age-related changes in CC tract density, we systematically compared four models: (1) linear (Age), (2) quadratic (Age + Age²), (3) logarithmic (log[Age]), and (4) cubic (Age +

$Age^2 + Age^3$). Model selection was based on Akaike Information Criterion (AIC), with lower values indicating better fit.

For each network, ordinary least squares regression models were fitted with harmonized tract density as the dependent variable, age terms (varying by model), sex, and site as covariates. Statistical significance was assessed using F-tests, with False Discovery Rate (FDR) correction applied across the seven networks ($q < 0.05$). All significant cubic age effects were validated using permutation testing (1000 iterations). Complete model comparison procedures, including permutation testing validation and FDR correction details, are provided in Supplementary Methods S4. Model comparison results for all networks are provided in Supplementary Table S3.

Correlation with cognitive and motor scores

To investigate relationships between CC tract density and cognitive/motor function, Pearson correlation analyses were performed for each of the seven functional networks with eight behavioral measures, resulting in 56 tests. All correlations were validated using permutation testing (10,000 iterations) to provide robust non-parametric significance estimates. Multiple comparison corrections were applied using both False Discovery Rate (FDR; Benjamini–Hochberg method) and Bonferroni procedures. Complete permutation testing procedures and validation metrics are detailed in Supplementary Methods S3. Full results for all 56 associations, including parametric and permutation-based p -values, effect sizes, and multiple comparison corrections, are provided in Supplementary Table S6.

Moderation analysis by age group

To test whether age moderates brain-behavior relationships, participants were divided into tertiles based on chronological age: Younger (36.0–51.75 years, $n = 239$), Middle (51.75–67.83 years, $n = 238$), and Older (67.92–100.0 years, $n = 241$). Linear regression models tested tract density \times age interactions for five networks (Somatomotor, Dorsal Attention, Salience/Ventral Attention, Control, Default) and three cognitive measures (TMT-A, TMT-B, RAVLT total recall), resulting in 15 tests. All interaction effects were validated using permutation testing (1000 iterations), with FDR correction applied across tests. Permutation procedures for interaction effects are detailed in Supplementary Methods S3.

To evaluate the robustness of age moderation findings to different grouping schemes, we conducted three sensitivity analyses using alternative age stratifications:

- Quartile-based grouping (4 groups): Participants divided into quartiles based on age distribution (Q1: 36.0–47.19 years, $N = 180$; Q2: 47.19–58.50 years, $N = 178$; Q3: 58.50–72.48 years, $N = 180$; Q4: 72.48–100.0 years, $N = 180$).

- Median split (2 groups): Participants divided at median age (Younger: 36.0–58.50 years, $N = 358$; Older: 58.50–100.0 years, $N = 360$).

- Continuous age interaction: ** No grouping; age treated as a continuous moderator in the interaction term (Tract Density \times Age(continues)).

For each approach, we repeated the same moderation analyses with permutation testing (1000 iterations) and FDR correction. Results were compared with the primary tertile-based analysis to assess consistency of findings across grouping schemes.

Quality control

Comprehensive quality control procedures were implemented to ensure data integrity. All 718 CC tracts underwent visual inspection to verify anatomical accuracy and proper midline crossing. Registration quality was assessed using automated correlation metrics. Fiber coherence indices were calculated to ensure reconstruction quality. Topology-informed pruning (32 iterations) was applied to remove false positive connections arising from crossing fibers or tracking artifacts. Complete quality control procedures, including registration quality metrics, and fiber coherence distributions, are detailed in Supplementary Methods S1. Quality control metrics for all subjects are provided in Supplementary Table S9 and Supplementary Figs. S9, S10.

Sensitive analysis

To assess robustness of findings across parcellation resolutions, we replicated the entire analysis pipeline using the higher-resolution Schaefer-Yeo 1000-node atlas. The 1000-node data underwent identical preprocessing, harmonization (ComBat with age and sex as protected covariates; Supplementary Methods S2), cubic polynomial modeling (Supplementary Methods S4), and brain-behavior correlation analyses with permutation testing (Supplementary Methods S3). Results comparing 400- and 1000-node parcellations are provided in Supplementary Tables S7, S8 and Supplementary Fig. S8.

Reporting summary

Further information on research design is available in the Nature Portfolio Reporting Summary linked to this article.

Data availability

The raw data analyzed in this study were obtained from the Human Connectome Project-Aging (HCP-A) Lifespan 2.0 Release and are available through the HCP website (<https://www.humanconnectome.org/study/hcp-lifespan-aging>). The fib files for tractography are available at https://brain-labsolver.org/hcp_a.html.

Received: 12 August 2025; Accepted: 10 November 2025;

Published online: 21 November 2025

References

1. Bloom, J. S. & Hynd, G. W. The role of the corpus callosum in interhemispheric transfer of information: excitation or inhibition? *Neuropsychol. Rev.* **15**, 59–71 (2005).
2. Syrmos, N., Giannouli, V., Kottas, S. & Turgut, M. History of the Corpus Callosum. In *The Corpus Callosum* (eds. Turgut, M., Tubbs, R. S., Turgut, A. T. & Bui, C. C. J.) 3–15 (Springer International Publishing, 2023). https://doi.org/10.1007/978-3-031-38114-0_1.
3. Thiebaut De Schotten, M. & Forkel, S. J. The emergent properties of the connected brain. *Science* **378**, 505–510 (2022).
4. Danielsen, V. M. et al. Lifespan trajectories of relative corpus callosum thickness: Regional differences and cognitive relevance. *Cortex* **130**, 127–141 (2020).
5. Delvenne, J.-F. & Malloy, E. Functional implications of age-related atrophy of the corpus callosum. *Neurosci. Biobehav. Rev.* **169**, 105982 (2025).
6. Westerhausen, R. et al. Comparative morphology of the corpus callosum across the adult lifespan in chimpanzees (*PAN TROGLODYTES*) and humans. *J. Comp. Neurol.* **529**, 1584–1596 (2021).
7. Westerhausen, R. & Meguerditchian, A. Corpus callosum morphology across the lifespan in baboons (*Papio anubis*): A cross-sectional study of relative mid-sagittal surface area and thickness. *Neurosci. Res.* **171**, 19–26 (2021).
8. Martins-Costa, C. & Knoblich, J. A. Corpus Callosum Evolution and Development. In *Neocortical Neurogenesis in Development and Evolution* (ed. Huttner, W.) 283–316 (Wiley, 2023). <https://doi.org/10.1002/9781119860914.ch15>.
9. Xiong, Y. et al. Cortical mapping of callosal connections in healthy young adults. *Hum. Brain Mapp.* **45**, e26629 (2024).
10. Forkel, S. J., Friedrich, P., Thiebaut De Schotten, M. & Howells, H. White matter variability, cognition, and disorders: a systematic review. *Brain Struct. Funct.* **227**, 529–544 (2022).
11. Malloy, E. & Delvenne, J.-F. Investigating the effects of ageing on interhemispheric communication using visual short-term memory binding. Preprint at <https://doi.org/10.31234/osf.io/6srhv> (2024).
12. Ribeiro, M., Yordanova, Y. N., Noblet, V., Herbet, G. & Ricard, D. White matter tracts and executive functions: a review of causal and correlation evidence. *Brain* **147**, 352–371 (2024).

13. Yeh, F.-C. Population-based tract-to-region connectome of the human brain and its hierarchical topology. *Nat. Commun.* **13**, 4933 (2022).
14. Fortin, J.-P. et al. Harmonization of cortical thickness measurements across scanners and sites. *NeuroImage* **167**, 104–120 (2018).
15. Acosta-Franco, J. A., Little, G. & Beaulieu, C. High resolution diffusion tensor imaging of the human cortex reveals non-linear trajectories over the healthy lifespan. *Imaging Neurosci.* **3**, IMAG.a.115 (2025).
16. Chen, X. et al. Lifespan trajectories of the morphology and tractography of the corpus callosum: a 5.0 T MRI study. *Brain Res.* **1850**, 149413 (2025).
17. Zhou, X. et al. Altered callosal morphology in post-stroke cognitive impairment. *Brain Res.* **1847**, 149307 (2025).
18. Griffis, J. C., Metcalf, N. V., Corbetta, M. & Shulman, G. L. Structural disconnections explain brain network dysfunction after stroke. *Cell Rep.* **28**, 2527–2540.e9 (2019).
19. Dong, Y. et al. How aging impacts cortical dynamics and gait during dual-task turning revealed by fNIRS. *GeroScience* <https://doi.org/10.1007/s11357-025-01687-6> (2025).
20. Karolis, V. R., Corbetta, M. & Thiebaut De Schotten, M. The architecture of functional lateralisation and its relationship to callosal connectivity in the human brain. *Nat. Commun.* **10**, 1417 (2019).
21. Rodríguez-Nieto, G. et al. Efficiency of structural brain networks mediates age-associated differences in executive functioning in older adults. *Front. Aging Neurosci.* **17**, 1593868 (2025).
22. Avvenuti, G. et al. Integrity of corpus callosum is essential for the cross-hemispheric propagation of sleep slow waves: a high-density EEG study in split-brain patients. *J. Neurosci.* **40**, 5589–5603 (2020).
23. Bookheimer, S. Y. et al. The lifespan human connectome project in aging: an overview. *NeuroImage* **185**, 335–348 (2019).
24. Harms, M. P. et al. Extending the human connectome project across ages: imaging protocols for the lifespan development and aging projects. *NeuroImage* **183**, 972–984 (2018).
25. Gershon, R. C. et al. NIH toolbox for assessment of neurological and behavioral function. *Neurology* **80**, s2–6 (2013).
26. Jenkinson, M., Beckmann, C. F., Behrens, T. E. J., Woolrich, M. W. & Smith, S. M. F. S. L. *NeuroImage* **62**, 782–790 (2012).
27. Yeh, F.-C. & Tseng, W.-Y. I. NTU-90: a high angular resolution brain atlas constructed by q-space diffeomorphic reconstruction. *NeuroImage* **58**, 91–99 (2011).
28. Yeh, F.-C. et al. Population-averaged atlas of the macroscale human structural connectome and its network topology. *NeuroImage* **178**, 57–68 (2018).
29. Yeh, F.-C. Shape analysis of the human association pathways. *NeuroImage* **223**, 117329 (2020).
30. Schaefer, A. et al. Local-global parcellation of the human cerebral cortex from intrinsic functional connectivity MRI. *Cereb. Cortex* **28**, 3095–3114 (2018).
31. Thomas Yeo, B. T. et al. The organization of the human cerebral cortex estimated by intrinsic functional connectivity. *J. Neurophysiol.* **106**, 1125–1165 (2011).

Author contributions

M.H.A.: methodology, design, conceptualization, formal analysis, statistics, interpretation, data visualization and writing of the draft.

Competing interests

The author declare no competing interests.

Informed consent

Informed consent was obtained from all participants according to the protocols approved by the Institutional Review Board (IRB) overseeing the Human Connectome Project.

Additional information

Supplementary information The online version contains supplementary material available at <https://doi.org/10.1038/s42003-025-09219-w>.

Correspondence and requests for materials should be addressed to Mohammad Hadi Aarabi.

Peer review information *Communications Biology* thanks Virendra Mishra and the other, anonymous, reviewer(s) for their contribution to the peer review of this work. Primary Handling Editors: Sahar Ahmad and Jasmine Pan. A peer review file is available.

Reprints and permissions information is available at <http://www.nature.com/reprints>

Publisher's note Springer Nature remains neutral with regard to jurisdictional claims in published maps and institutional affiliations.

Open Access This article is licensed under a Creative Commons Attribution-NonCommercial-NoDerivatives 4.0 International License, which permits any non-commercial use, sharing, distribution and reproduction in any medium or format, as long as you give appropriate credit to the original author(s) and the source, provide a link to the Creative Commons licence, and indicate if you modified the licensed material. You do not have permission under this licence to share adapted material derived from this article or parts of it. The images or other third party material in this article are included in the article's Creative Commons licence, unless indicated otherwise in a credit line to the material. If material is not included in the article's Creative Commons licence and your intended use is not permitted by statutory regulation or exceeds the permitted use, you will need to obtain permission directly from the copyright holder. To view a copy of this licence, visit <http://creativecommons.org/licenses/by-nc-nd/4.0/>.

© The Author(s) 2025